Published in final edited form as:

Nature. 2010 January 7; 463(7277): 98–102. doi:10.1038/nature08652.

High-Performance Genetically Targetable Optical Neural Silencing via Light-Driven Proton Pumps

Brian Y. Chow[(†),1,2], **Xue Han**[(†),1,2], **Allison S. Dobry**[1,2], **Xiaofeng Qian**[1,2], **Amy S. Chuong**[1,2], **Mingjie Li**[1,2], **Michael A. Henninger**[1,2], **Gabriel M. Belfort**[2], **Yingxi Lin**[2], **Patrick E. Monahan**[1,2], and **Edward S. Boyden**[(*),1,2]

[1]The MIT Media Laboratory, Synthetic Neurobiology Group, and Department of Biological Engineering, Massachusetts Institute of Technology, Cambridge, MA 02139

[2]Department of Brain and Cognitive Sciences and MIT McGovern Institute for Brain Research, Massachusetts Institute of Technology, Cambridge, MA 02139

Abstract

The ability to silence the activity of genetically specified neurons in a temporally precise fashion would open up the ability to investigate the causal role of specific cell classes in neural computations, behaviors, and pathologies. Here we show that members of the class of light-driven outward proton pumps can mediate very powerful, safe, multiple-color silencing of neural activity. The gene archaerhodopsin-31 (Arch) from *Halorubrum sodomense* enables near-100% silencing of neurons in the awake brain when virally expressed in mouse cortex and illuminated with yellow light. Arch mediates currents of several hundred picoamps at low light powers, and supports neural silencing currents approaching 900 pA at light powers easily achievable *in vivo*. In addition, Arch spontaneously recovers from light-dependent inactivation, unlike light-driven chloride pumps that enter long-lasting inactive states in response to light. These properties of Arch are appropriate to mediate the optical silencing of significant brain volumes over behaviourally-relevant timescales. Arch function in neurons is well tolerated because pH excursions created by Arch illumination are minimized by self-limiting mechanisms to levels comparable to those mediated by channelrhodopsins2,3 or natural spike firing. To highlight how proton pump ecological and genomic diversity may support new innovation, we show that the blue-green light-drivable proton pump from the fungus *Leptosphaeria maculans*4 (Mac) can, when expressed in neurons, enable neural silencing by blue light, thus enabling alongside other developed reagents

(*)Correspondence and requests for materials should be addressed to E.S.B. (esb@media.mit.edu)..

Authors' Contributions B.Y.C., X.H., and E.S.B. designed experiments, analyzed data, and wrote the paper. B.Y.C. and X.H. carried out experiments. A.S.D. assisted with electrophysiological recording. X.Q., M.L., and A.S.C. assisted with molecular biology, virus making, and transfections. M.A.H. performed Monte Carlo modelling. P.E.M., G.M.B., and Y.L. created hippocampal and cortical neural cultures.

(†)These authors contributed equally to this work.

Supplementary Information accompanies the paper on www.nature.com/nature

GENBANK (http://www.ncbi.nlm.nih.gov/) accession numbers: mammalian codon-optimized Arch, GU045593; mammalian codon-optimized Arch fused to GFP, GU045594; mammalian codon-optimized Mac, GU045595; mammalian codon-optimized Mac fused to GFP, GU045596; ss-Prl-Arch, GU045597; ss-Arch-GFP-ER2, GU045598; ss-Prl-Arch-GFP, GU045599.

The authors declare no competing financial interests.

the potential for independent silencing of two neural populations by blue vs. red light. Light-driven proton pumps thus represent a high-performance and extremely versatile class of "optogenetic" voltage and ion modulator, which will broadly empower new neuroscientific, biological, neurological, and psychiatric investigations.

We screened type I microbial opsins (see Supplementary Table 1) from archaebacteria, bacteria, plants, and fungi for light-driven hyperpolarizing capability. Mammalian codon-optimized genes were synthesized, cloned into GFP-fusion expression vectors, and transfected into cultured neurons. We measured opsin photocurrents and cell capacitance-normalized photocurrent densities under stereotyped illumination conditions (Fig. 1A, black and gray bars respectively), as well as opsin action spectra (photocurrent as a function of wavelength; Supplementary Table 2). From this information, we estimated the photocurrent density for each opsin at its own spectral peak (Fig. 1A, white bars). For comparison purposes, we included an earlier-characterized microbial opsin, the *Natronomonas pharaonis* halorhodopsin (Halo/NpHR), a light-driven inward chloride pump capable of modest hyperpolarizing currents5–8. Archaerhodopsin-3 from *Halorubrum sodomense* (Arch/aR-3), hypothesized to be a proton pump1, generated large photocurrents in the screen, as did two other proton pumps, the *Leptosphaeria maculans* opsin (Mac/LR/Ops)4 and cruxrhodopsin-19 (albeit less than that of Arch; Fig. 1A). All light-driven chloride pumps assessed had lower screen photocurrents than these light-driven proton pumps.

Arch is a yellow-green light sensitive (Fig. 1B) opsin which appears to express well on the neural plasma membrane (Fig. 1C; see Supplementary Notes on Arch expression levels and enhancing Arch membrane trafficking). Arch-mediated currents exhibited excellent kinetics of light-activation and post-light recovery. Upon illumination, Arch currents rose with a 15%–85% onset time of 8.8 ± 1.8 ms (mean ± standard error (SE) reported throughout, unless otherwise indicated; N = 16 neurons), and after light cessation, Arch currents fell with an 85%–15% offset time of 19.3 ± 2.9 ms. Under continuous yellow illumination, Arch photocurrent declined (Fig. 1D, 1E), as did the photocurrents of all of the opsins in our screen. However, unlike all of the halorhodopsins we screened (including products of halorhodopsin site-directed mutagenesis aimed at improving kinetics, Supplementary Table 3), which after illumination remained inactivated for long periods of time (e.g., tens of minutes, with accelerated recovery requiring additional blue light5,10). Arch spontaneously recovered function in seconds (Fig. 1D, 1E), more like the light-gated cation channel channelrhodopsin-2 (ChR2)2,3. The magnitude of Arch-mediated photocurrents was large. At low light irradiances of 0.35 and 1.28 mW/mm^2 (Fig. 1Fi), neural Arch currents were 120 and 189 pA respectively; at higher light powers (e.g., at which Halo currents saturate), Arch currents continued to increase, approaching 900 pA at effective irradiances of 36 mW/mm^2, well within the reach of typical *in vivo* experiments (Fig. 1Fii; see **Methods** for how effective irradiances were calculated). The high dynamic range of Arch may enable excellent utilization of light sources (e.g., LEDs, lasers) that are safe and effective for optical control *in vivo*11,12.

Several lines of evidence supported the idea that Arch functioned as an outward proton pump when expressed in neurons. Removing the endogenous ions that commonly subserve

neural inhibition, Cl^- and K^+, from physiological solutions did not alter photocurrent magnitude ($p > 0.4$ comparing either K^+ free or Cl^- free solutions to regular solutions, t-test; Fig. 2A). In solutions lacking Na^+, K^+, Cl^-, and Ca^{2+}, photocurrents were still no different from those measured in normal solutions ($p > 0.4$; N = 4 neurons tested without these four charge carriers). The reversal potential appeared to be less than −120 mV (Fig. 2B), also consistent with Arch being a proton pump.

We assessed the voltage swings driven by illumination of current-clamped Arch-expressing cultured neurons. As effective irradiance increased from 7.8 mW/mm^2 to 36.3 mW/mm^2 (Fig. 1F), voltage clamped neurons exhibited peak currents that increased from 350 ± 35 pA (N = 16 neurons) to 863 ± 62 pA (N = 8 neurons) respectively. Current-clamped neurons under these two irradiance conditions were hyperpolarized by −69.6 ± 7.3 mV (N = 10) and −76.2 ± 10.1 mV (N = 8) respectively. Surprisingly, these voltage deflections, while both large, were not significantly different from one another ($p > 0.7$, t-test), suggesting the existence of a rapidly activated transporter or exchanger (perhaps the Na^+-dependent Cl^-/HCO_3^- exchanger), or the opening of hyperpolarization-gated channels capable of shunting protons, which limit the effects of Arch on accumulated proton (or other charge carrier) gradients across neural membranes. This enabling of effective but not excessive silencing may make Arch safer than pumps that accumulate ions without self-regulation.

We next assessed the changes in intracellular pH (pH_i) driven by illumination of Arch-expressing cultured neurons, using the fluorescent pH indicator carboxy-SNARF-1. Within one second of illumination with strong green light (Fig. 2C), pH_i rose from 7.309 ± 0.011 to 7.431 ± 0.020, plateauing rapidly. pH_i increased slightly further after 15 s of illumination, to 7.461 ± 0.024 (Fig. 1E). The fast stabilization of pH_i may reflect the same self-limiting influence that limits proton-mediated voltage swings as described above, and may contribute to the safe operation of Arch in neurons by preventing large pH_i swings. The changes in pH_i observed here are comparable in magnitude to those observed during illumination of ChR2-expressing cells13 (due to the proton currents carried by ChR23,14) and are also within the magnitudes of changes observed during normal neural activity15–18. Passive electrical properties of neurons were not affected by Arch expression (Fig. 2E–G; $p > 0.6$ for each measure, t-test), nor was cell death ($p > 0.6$, $\chi^2 = 0.26$; Fig. 2D).

We estimated the tissue volumes that could be silenced, using *in vitro* experiments and computational modeling. In cultured neurons expressing Arch or a trafficking-improved variant of Halo, eNpHR7,8, we somatically injected brief current pulses at magnitudes chosen to mimic the current drives of neurons in the intact nervous system19–22. We exposed these neurons to periods of 575 nm yellow light (0.35, 1.28, or 6 mW/mm^2, simulating irradiance ~1.7, 1.2, or 0.6 mm away from the tip of a 200 micron fiber emitting 200 mW/mm^2 irradiance, as modelled by Monte Carlo methods; see Supplementary Figure 3), and measured the reduction in spike rate for each condition (Fig. 3A). In general, Arch-expressing neurons were significantly more inhibited than eNpHR-expressing cells. According to our model and the 350 pA data in Fig. 3A, the increase in brain tissue volume that would be 45–55% optically silenced would be ~10x larger for Arch than for eNpHR.

To directly assess Arch *in vivo*, we injected lentivirus encoding for Arch into mouse cortex and recorded neural responses ~1 month later. Arch expressed well (Fig. 3Bi) and appeared well localized to the plasma membrane, labeling cell bodies, processes, and dendritic spines (Fig. 3Bii). We recorded neurons in awake headfixed mice, illuminating neurons via a 200 micron optical fiber coupled to a 593 nm laser (power at electrode tip estimated at ~3 mW/mm^2 11,12,23). Upon light onset, firing rates of many units immediately and strongly declined, and remained low throughout the period of illumination, for both brief (Fig. 3Ci, ii, 3D) and long (Fig. 3Ciii, iv) pulses. We recorded 13 single units which showed any decrease in firing during illumination, objectively identified as described in the **Methods**, and found spiking rates during exposure to 5 s yellow light (Fig. 3D) to drop by an average of 90 ± 15% (mean ± standard deviation (SD); Fig. 3E, 3F), restoring to levels indistinguishable from baseline after light cessation ($p > 0.2$, paired t-test; Fig. 3F). 6 of the 13 units decreased spike rate by at least 99.5%, and the median decrease was 97.1% (Fig. 3G). One possibility is that Arch-expressing cells were almost completely silenced, whereas non-infected cells decreased activity due to network activity reduction during illumination; note that only excitatory cells were genetically targeted here. Optical silencing was consistent across trials ($p > 0.1$, paired t-test comparing, for each neuron, responses to first 3 vs. last 3 light exposures; ~20 trials per neuron). The kinetics of silencing were rapid: for the 6 neurons that underwent >99.5% silencing, spike firing reduced with near-0 ms latency, rarely firing spikes after light onset; averaged across all cells, firing rate reductions plateaued within 229 ± 310 ms after light onset (mean ± SD). After light cessation, firing rate restored quickly for the highly-silenced neurons; averaged across all cells, firing rates took 355 ± 505 ms to recover after light offset. The level of post-light firing did not vary with repeated light exposure ($p > 0.7$, paired t-test comparing, for each neuron, after-light firing rates during first 3 vs. the last 3 trials). Thus, Arch could mediate reliable, near-digital silencing of neurons in the awake mammalian brain.

Proton pumps naturally exist that are activated by many colors of light (see Supplementary Table 1), in contrast to chloride pumps, which are primarily driven by yellow-orange light (even with significant mutagenesis of retinal-flanking residues, Supplementary Table 3). The light-driven proton pump Mac (Fig. 1A), in our screen, had an action spectrum strongly blueshifted relative to that of the light-driven chloride pump Halo (Fig. 4A). We found that Mac-expressing neurons could undergo 4.1-fold larger hyperpolarizations with blue light than with red light, and Halo-expressing neurons could undergo 3.3-fold larger hyperpolarizations with red light than with blue light, when illuminated with appropriate filters (Fig. 4B). Accordingly, we could demonstrate selective silencing of spike firing in Mac-expressing neurons in response to blue light, and selective silencing of spike firing in Halo-expressing neurons in response to red light (Fig. 4C). Thus, the spectral diversity of proton pumps points the way towards independent multi-color silencing of separate neural populations. This result opens up novel kinds of experiment, in which, for example, two neuron classes, or two sets of neural projections from a single site, can be independently silenced during a behavioral task.

Arch and Mac represent members of a new, diverse, and powerful class of optical neural silencing reagent, the light-driven proton pump, which operates without the need for

exogenous chemical supplementation in mammalian cells. The efficacy of these proton pumps is surprising, given that protons occur, in mammalian tissue, at a millionfold-lower concentration than the ions carried by other optical control molecules. This high efficacy may be due to the fast photocycle of Arch (see also 24,25), but it may also be due to the ability of high-pKa residues in proton pumps to mediate proton uptake24,26. We discovered several facts about this class of molecules that point the way for future neuroengineering innovation. First, proton pumping is a self-limiting process in neurons, providing for a safe and naturalistic form of neural silencing. Second, proton pumps recover spontaneously after optical activation, improving their relevance for behaviourally-relevant silencing over the class of halorhodopsins. Finally, proton pumps exist with a wide diversity of action spectra, thus enabling multiple-color silencing of distinct neural populations. Structure-guided mutagenesis of Arch and Mac may further facilitate development of neural silencers with altered spectrum or ion selectivity, given the significant amount of structure-function knowledge of the proton pump family (e.g., 27–29).

Our study highlights the importance of ecological and genomic diversity in providing novel molecular reagents for optical control of biological processes, as has previously benefited the fluorescent protein community. These opsins are likely to find uses across the spectrum of neuroscientific, biological, and bioengineering fields. For example, expression of these opsins in neurons, muscle, immune cells, and other excitable cells will allow control over their membrane potential, opening up the ability to investigate the causal role of specific cells' activities in intact organisms, and opening up the ability to understand the causal contribution of such cells to disease states in animal models. With the recent demonstration of the safe and efficacious use of the microbial opsin ChR2 to control neurons in non-human primates23, it is in principle possible that in the future, these opsins may subserve new forms of neuromodulation technology that bear clinical benefit.

Methods Summary

See Supplementary Methods for detailed methods. Constructs with Arch, Mac, and Halo are available at http://syntheticneurobiology.org/protocols. In brief, codon-optimized genes were synthesized by Genscript and fused to GFP in lentiviral and mammalian expression vectors as used previously5,23 for transfection or viral infection of neurons. Primary hippocampal or cortical neurons were cultured and then transfected with plasmids or infected with viruses encoding for genes of interest, as described previously5. Images were taken using a Zeiss LSM 510 confocal microscope. Patch clamp recordings were made using glass microelectrodes and a Multiclamp 700B/Digidata electrophysiology setup, using appropriate pipette and bath solutions for the experimental goal at hand. Neural pH imaging was done using carboxy-SNARF-1-AM ester (Invitrogen). Cell health was assayed using Trypan blue staining (Gibco). HEK cells were cultured and patch clamped using standard protocols. Mutagenesis was performed using the QuikChange kit (Stratagene). Computational modelling of light propagation was done with Monte Carlo simulation with MATLAB. *In vivo* recordings were made on headfixed awake mice, which were surgically injected with lentivirus, and implanted with a headplate as described before23. Glass pipettes attached to laser-coupled optical fibers were inserted into the brain, to record neural activity during laser illumination in a photoelectrochemical artifact-free way. Data analysis

was performed using Clampfit, Excel, Origin, and MATLAB. Histology was performed using transcardial formaldehyde perfusion followed by sectioning and subsequent confocal imaging.

Supplementary Material

Refer to Web version on PubMed Central for supplementary material.

Acknowledgments

ESB acknowledges funding by the NIH Director's New Innovator Award (DP2 OD002002-01), as well as by the NSF (0835878 and 0848804), the McGovern Institute Neurotechnology Award Program, the Department of Defense, NARSAD, the Alfred P. Sloan Foundation, Jerry and Marge Burnett, the SFN Research Award for Innovation in Neuroscience, the MIT Media Lab, the Benesse Foundation, and the Wallace H. Coulter Foundation. XH acknowledges the Helen Hay Whitney Foundation and NIH 1K99MH085944. The authors thank Eva Klinman for help with transfections, Robert Desimone for advice, John Lin for technical aid on intracellular pH measurements, Kunio Ihara for discussions about archaerhodopsins, and Michael Hemann and Neil Gershenfeld and the Center for Bits and Atoms for use of their respective lab facilities.

REFERENCES

1. Ihara K, et al. Evolution of the archaeal rhodopsins: evolution rate changes by gene duplication and functional differentiation. J Mol Biol. 1999; 285:163–174. [PubMed: 9878396]
2. Boyden ES, Zhang F, Bamberg E, Nagel G, Deisseroth K. Millisecond-timescale, genetically targeted optical control of neural activity. Nat Neurosci. 2005; 8:1263–1268. [PubMed: 16116447]
3. Nagel G, et al. Channelrhodopsin-2, a directly light-gated cation-selective membrane channel. Proc Natl Acad Sci U S A. 2003; 100:13940–13945. [PubMed: 14615590]
4. Waschuk SA, Bezerra AG, Shi L, Brown LS. Leptosphaeria rhodopsin: Bacteriorhodopsin-like proton pump from a eukaryote. Proceedings of the National Academy of Sciences of the United States of America. 2005; 102:6879–6883. doi:10.1073/pnas.0409659102. [PubMed: 15860584]
5. Han X, Boyden ES. Multiple-color optical activation, silencing, and desynchronization of neural activity, with single-spike temporal resolution. PLoS ONE. 2007; 2:e299. [PubMed: 17375185]
6. Zhang F, et al. Multimodal fast optical interrogation of neural circuitry. Nature. 2007; 446:633–639. [PubMed: 17410168]
7. Zhao S, et al. Improved expression of halorhodopsin for light-induced silencing of neuronal activity. Brain cell biology. 2008; 36:141–154. [PubMed: 18931914]
8. Gradinaru V, Thompson KR, Deisseroth K. eNpHR: a Natronomonas halorhodopsin enhanced for optogenetic applications. Brain cell biology. 2008; 36:129–139. [PubMed: 18677566]
9. Tateno M, Ihara K, Mukohata Y. The novel ion pump rhodopsins from Haloarcula form a family independent from both the bacteriorhodopsin and archaerhodopsin families/tribes. Arch Biochem Biophys. 1994; 315:127–132. [PubMed: 7979388]
10. Bamberg E, Tittor J, Oesterhelt D. Light-driven proton or chloride pumping by halorhodopsin. Proc Natl Acad Sci U S A. 1993; 90:639–643. [PubMed: 8380643]
11. Aravanis AM, et al. An optical neural interface: in vivo control of rodent motor cortex with integrated fiberoptic and optogenetic technology. Journal of neural engineering. 2007; 4:S143–156. [PubMed: 17873414]
12. Bernstein JG, et al. Prosthetic systems for therapeutic optical activation and silencing of genetically-targeted neurons. Proceedings - Society of Photo-Optical Instrumentation Engineers. 2008; 6854:68540H.
13. Lin JY, Lin MZ, Steinbach P, Tsien RY. Characterization of engineered channelrhodopsin variants with improved properties and kinetics. Biophys J. 2009; 96:1803–1814. [PubMed: 19254539]
14. Berthold P, et al. Channelrhodopsin-1 Initiates Phototaxis and Photophobic Responses in Chlamydomonas by Immediate Light-Induced Depolarization. Plant Cell. 2008; 20:1665–1677. doi:10.1105/tpc.108.057919. [PubMed: 18552201]

15. Bevensee MO, Cummins TR, Haddad GG, Boron WF, Boyarsky G. pH regulation in single CA1 neurons acutely isolated from the hippocampi of immature and mature rats. J Physiol. 1996; 494(Pt 2):315–328. [PubMed: 8841993]
16. Chesler M. Regulation and modulation of pH in the brain. Physiological reviews. 2003; 83:1183–1221. [PubMed: 14506304]
17. Meyer TM, Munsch T, Pape HC. Activity-related changes in intracellular pH in rat thalamic relay neurons. Neuroreport. 2000; 11:33–37. [PubMed: 10683825]
18. Trapp S, Luckermann M, Brooks PA, Ballanyi K. Acidosis of rat dorsal vagal neurons in situ during spontaneous and evoked activity. J Physiol. 1996; 496(Pt 3):695–710. [PubMed: 8930837]
19. Leinekugel X, et al. Correlated bursts of activity in the neonatal hippocampus in vivo. Science. 2002; 296:2049–2052. [PubMed: 12065842]
20. Wehr M, Zador AM. Balanced inhibition underlies tuning and sharpens spike timing in auditory cortex. Nature. 2003; 426:442–446. [PubMed: 14647382]
21. Richter DW, Pierrefiche O, Lalley PM, Polder HR. Voltage-clamp analysis of neurons within deep layers of the brain. J Neurosci Methods. 1996; 67:121–123. [PubMed: 8872877]
22. Narikawa K, Furue H, Kumamoto E, Yoshimura M. In vivo patch-clamp analysis of IPSCs evoked in rat substantia gelatinosa neurons by cutaneous mechanical stimulation. J Neurophysiol. 2000; 84:2171–2174. [PubMed: 11024105]
23. Han X, et al. Millisecond-timescale optical control of neural dynamics in the nonhuman primate brain. Neuron. 2009; 62:191–198. [PubMed: 19409264]
24. Ming M, et al. pH dependence of light-driven proton pumping by an archaerhodopsin from Tibet: comparison with bacteriorhodopsin. Biophys J. 2006; 90:3322–3332. [PubMed: 16473896]
25. Lukashev EP, et al. pH dependence of the absorption spectra and photochemical transformations of the archaerhodopsins. Photochem Photobiol. 1994; 60:69–75. [PubMed: 8073078]
26. Lanyi JK. Proton transfers in the bacteriorhodopsin photocycle. Biochimica et Biophysica Acta (BBA) - Bioenergetics. 2006; 1757:1012–1018. [PubMed: 16376293]
27. Enami N, et al. Crystal structures of archaerhodopsin-1 and -2: Common structural motif in archaeal light-driven proton pumps. J Mol Biol. 2006; 358:675–685. [PubMed: 16540121]
28. Mogi T, Marti T, Khorana HG. Structure-function studies on bacteriorhodopsin. IX. Substitutions of tryptophan residues affect protein-retinal interactions in bacteriorhodopsin. J Biol Chem. 1989; 264:14197–14201. [PubMed: 2547787]
29. Luecke H, Schobert B, Richter HT, Cartailler JP, Lanyi JK. Structure of bacteriorhodopsin at 1.55 A resolution. J Mol Biol. 1999; 291:899–911. [PubMed: 10452895]

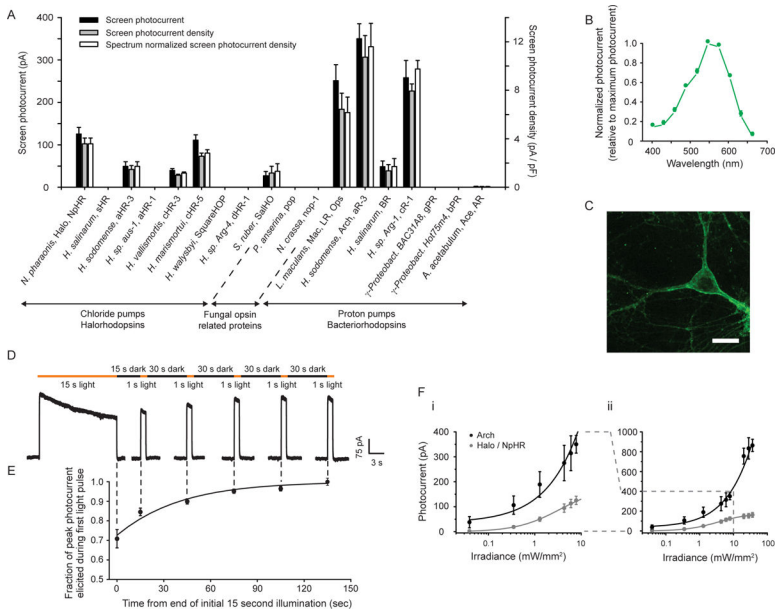

Figure 1.

Optical neural silencing via light-driven proton pumping, revealed by a cross-kingdom functional molecular screen. **(A)** Screen data showing outward photocurrents (left ordinate, black bars), photocurrent densities (right ordinate, gray bars), and action spectrum-normalized photocurrent densities (right ordinate, white bars), measured via whole-cell patch clamp of cultured neurons under screening illumination conditions (575±25 nm, 7.8 mW/mm^2 for all but Mac/LR/Ops, gPR, bPR, and Ace/AR, which were 535±25 nm, 9.4 mW/mm^2; see Supplementary Table 1 for details on the molecules screened; N = 4–16 neurons for each bar). All data in this and other figures are mean ± standard error (SE) unless otherwise indicated. **(B)** Action spectrum of Arch measured in cultured neurons by scanning illumination light wavelength through the visible spectrum (N = 7 neurons). **(C)** Confocal fluorescence image of a lentivirally-infected cultured neuron expressing Arch-GFP (scale bar, 20 μm). **(D)** Raw current trace of a neuron lentivirally-infected with Arch, illuminated by a 15 s light pulse (575 ± 25 nm, irradiance 7.8 mW/mm^2), followed by 1 s test pulses delivered starting 15, 45, 75, 105, and 135 seconds after the end of the 15 s light pulse. **(E)** Population data of averaged Arch photocurrents (N = 11 neurons) sampled at the times indicated by the vertical dotted lines that extend into **Fig. 1D**. **(F)** Photocurrents of Arch vs. Halo measured as a function of 575 ± 25 nm light irradiance (or effective light irradiance; see **Methods** for details), in patch-clamped cultured neurons (N = 4 – 16 neurons for each point), for low (**i**) and high (**ii**) light powers. The line is a single Hill fit to the data.

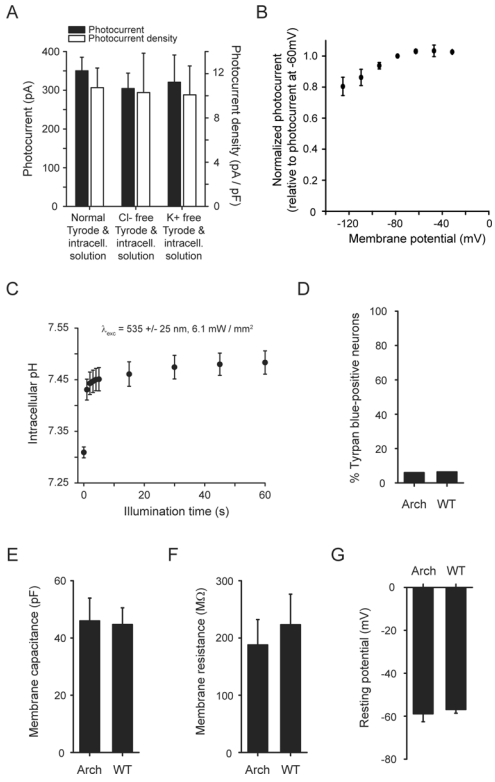

Figure 2.

Functional properties of the light-driven proton pump Arch in neurons. (**A**) Photocurrent of Arch measured as a function of ionic composition (575 ± 25 nm light, 7.8 mW/mm^2), showing no significant dependence of photocurrent on concentration of Cl− or K+ ions (N = 16, 8 and 7 neurons, from left to right). **(B)** Arch proton photocurrent vs. holding potential (N = 4 neurons). (**C**) Intracellular pH measurements over a one minute period of continuous illumination and simultaneous imaging (535 ± 25 nm light, 6.1 mW/mm^2,) using SNARF-1 pH-sensitive ratiometric dye (N = 10 – 20 cells per datapoint). **(D)** Trypan blue staining of neurons lentivirally-infected with Arch vs. wild-type (WT) neurons, measured at 18 days *in vitro* (N = 669 Arch-expressing, 512 wild-type, neurons). **(E)** Membrane capacitance, **(F)** membrane resistance, and **(G)** resting potential in neurons lentivirally-infected with Arch vs. wild-type (WT) neurons, measured at 11 days *in vitro* (N = 7 cells each).

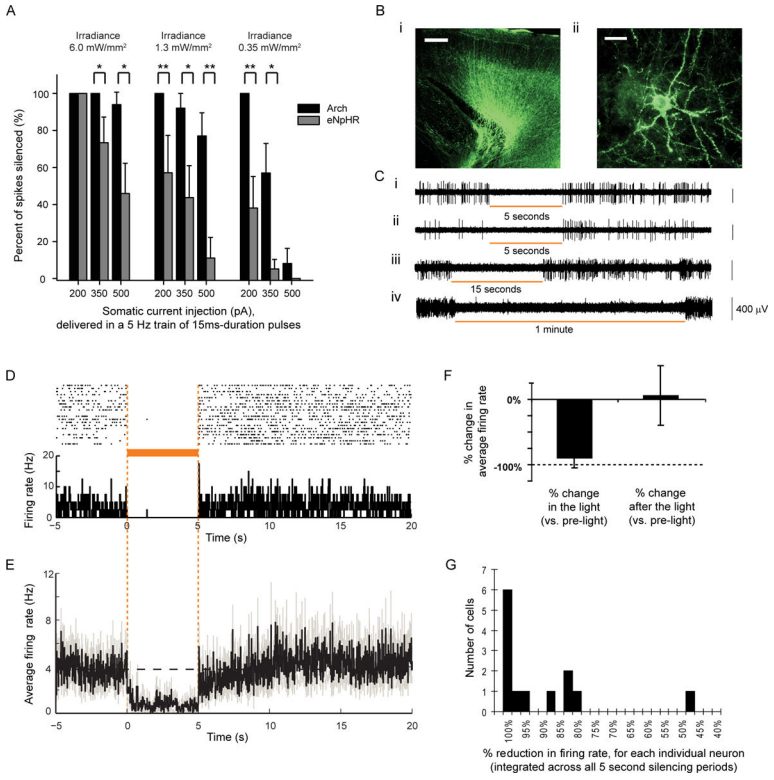

Figure 3.

High-performance Arch-mediated optical neural silencing of neocortical regions in awake mice. (**A**) *In vitro* data showing, in cultured neurons expressing Arch or eNpHR and receiving trains of somatic current injections (15 ms pulse durations at 5 Hz), the percent reduction of spiking under varying light powers (575 ± 25 nm light) as might be encountered *in vivo*. *, $p < 0.05$; **, $p < 0.01$, t-test. N = 7–8 cells for each condition. (**B**) Fluorescence images showing Arch-GFP expression in mouse cortex ~1 month after lentiviral injection (**i**; scale bar, 200 µm, **ii**, 20 µm. (**C**) Representative extracellular recordings showing neurons undergoing 5-second (**i, ii**), 15-second (**iii**), and 1-minute (**iv**) periods of light illumination (593 nm; ~150 mW/mm^2 radiant flux out the fiber tip; and expected to be ~3 mW/mm^2 at the electrode tip ~800 um away11,12,23). (**D**) Neural activity in a representative neuron before, during, and after 5 seconds of yellow light illumination, shown as a spike raster plot (top), and as a histogram of instantaneous firing rate averaged across trials (bottom; bin size, 20 ms). (**E**) Population average of instantaneous firing rate before, during and after yellow light illumination (black line, mean; gray lines, mean ± SE; n = 13 units). (**F**) Average change in spike firing during 5 seconds of yellow light illumination (left) and during the 5 seconds immediately after light offset (right), for the data shown in **D**. (**G**) Histogram of percentage reductions in spike rate.

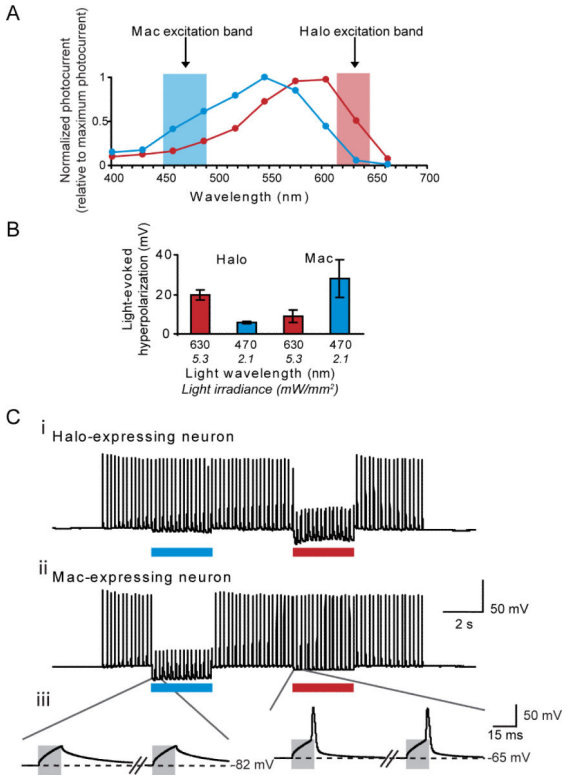

Figure 4.

Multicolor silencing of two neural populations, enabled by blue- and red-light drivable ion pumps of different classes. (**A**) Action spectra of Mac vs. Halo; rectangles indicate filter bandwidths used for multi-color silencing *in vitro*. Blue light power is via a 470 ± 20 nm filter at 5.3 mW/mm^2, and red light power is via a 630 ± 15 nm filter at 2.1 mW/mm^2. (**B**) Membrane hyperpolarizations elicited by blue vs. red light, in cells expressing Halo or Mac (N = 5 Mac-expressing neurons, N = 6 Halo-expressing neurons). (**C**) Action potentials evoked by current injection into patch clamped cultured neurons transfected with Halo (**i**) were selectively silenced by the red light but not by the blue light, and vice-versa in neurons expressing Mac (**ii**). Gray boxes in the inset (**iii**) indicate periods of patch clamp current injection.